

SIMULATIONS OF ROUGHNESS-SALINITY-TEMPERATURE ANOMALIES AT S-L-BANDS

Victor Raizer

Zel Technologies, LLC, Fairfax, VA 22032, USA
Telephone: 703 764 2308; e-mail: vraizer@aol.com

ABSTRACT

We report a novel class of ocean remote-sensing signatures associated with so-called “roughness-salinity-temperature anomalies” (RSTA). Oceanic RSTA can occur in restricted areas under the influence of joint variations of surface roughness, surface salinity, and temperature. The most probable environmental causes are interactions between thermohaline and wave processes. To provide an appropriate study, we develop numerical simulations of possible radiometric signals, images, and features. For this goal, we have used a composite multifactor hydrodynamic-electromagnetic model developed in our previous work. Examples of radiometric signatures related to RSTA will be demonstrated. We also point out possibilities for their observations using advanced passive microwave techniques. These results will be presented and explained.

Index Terms—Remote sensing, microwave radiometry, salinity, sea surface

1. INTRODUCTION

During the last three decades, the value of passive microwave techniques for diagnostics of oceanic processes and fields has been demonstrated. Indeed, S-L-band radiometers provide day/night monitoring of the ocean surface under practically any weather conditions. Atmospheric effects, contributions from clouds, precipitations, and snow can be neglected in most environmental situations. Thus, S-L-band microwave radiometry and imagery have potential capabilities to observe sophisticated ocean surface phenomena directly. Because at S-L-band the thickness of the electromagnetic skin layer can reach several centimeters depending on dielectric permittivity, temperature, and salinity of seawater, it is possible to monitor the variability of the ocean subsurface layer as a whole hydrodynamic system. As shown in previous work (e.g., [1]), surface roughness, foam/whitecap, subsurface bubbles, spray/aerosol, salinity, and temperature are the main factors affecting on ocean emissivity. These issues were updated and reported in [2] – [6].

Experimental oceanographic data show that the upper layer of the ocean, including the air-water interface and thin electromagnetic skin layer (at S-L-band), is usually unstable and nonuniform. These conditions may occur under the influence of different environmental processes [7], [8]: thermohaline (i.e. joint salinity, temperature, and density) circulations, double-diffusive and convective processes, turbulent mixing, hydrodynamic interactions, wave modulations, currents, wave breaking, and wind actions. In this context, natural RSTA are abundant, fascinating,

and important geophysical phenomena. As we know the most probable surface manifestations of RSTA can be the following: 1) a double-diffusive instability called “salt fingers” (e.g., [9], [10]), 2) temperature fronts, thermohaline “wakes”, saltwater intrusions, or freshwater injections, and 3) strong rip current events referred to as “suloy” [11]. Fig. 1 illustrates the ocean observation environment in the presence of these listed phenomena. To describe the electromagnetic properties of the surface in such situations, we employ a composite multifactor model allowing estimation and prediction of possible microwave emission signatures. In this paper we present our data modeling.

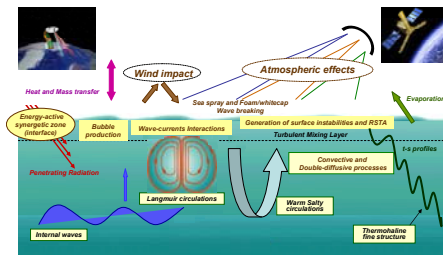


Fig. 1. Natural phenomena and mechanisms causing RSTA.

2. BASIC DESCRIPTION

A composite model is a model that contains several model partitions. In our case, the selected partitions are connected stochastically using probability rules. Each model partition is computed separately. The basic concept of our modeling is shown in Fig. 2.

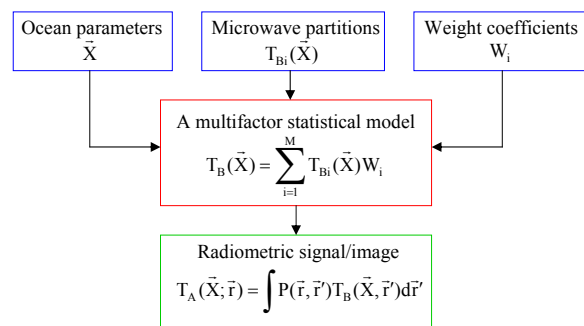


Fig. 2. Basic model concept.

This model operates with a vector of ocean parameters $\vec{X} = \{E(\vec{k}, \omega), \tilde{\omega}, \tilde{x}, v, t, s; d_f\}$ which are the following: wave spectrum $E(\vec{k}, \omega)$, dimensionless spectral peak $\tilde{\omega}$, dimensionless fetch \tilde{x} , wind speed v , temperature t , salinity s , and structural characteristics of dispersed media (foam/whitecap/spray/bubbles) d_f . To compute the total value of brightness temperature $T_B(\vec{X})$, we sum microwave partitions $T_{Bi}(\vec{X})$ with weight coefficients W_i describing contributions from the i -factor ($i = 1, \dots, M$; M is the number of participating factors). We take also into account an observation process, i.e., the relationship between desired antenna brightness temperature $T_A(\vec{X}, \vec{r})$ and actual brightness temperature $T_B(\vec{X})$ computed by a multifactor microwave emission model; $P(\vec{r}, \vec{r}')$ is the point spread function. Finally, we have adapted a basic model (Fig. 2) into digital format providing computer simulations of radiometric signals and images.

3. FRAMEWORK

Since 1998 we have developed digital techniques for analysis and modeling of high-resolution multiband ocean microwave radiometric images and signals including averaging, convolution, filtering, feature extraction, and mapping operations with the brightness-temperature fields (referred to as “radio-brightness”). Selected results have been published in [12] – [17]. To generate stochastic realizations, we have employed the following mathematical random field models: 1) Brownian motion random field (BRF), 2) Gaussian random field (GRF), 3) Markov random field (MRF), and 4) Self-similar, fractal (FRF).

In all cases, ocean passive microwave images can be modeled as discrete two-dimensional random fields of radio-brightness using statistical characterization and linear matrix formulation (described, e.g., in [18]). However, uncertainties may occur in the geophysical interpretation of these computer-generated microwave images because of their parameterized complexity and low signal-to-noise ratio. In the simplified case, an output image can be expressed in the product form $\Delta T_A = \Delta T_B \otimes H_p + \eta$, where ΔT_A and ΔT_B are matrixes representing desired (averaged) and actual (“pixel”) brightness-temperature contrasts, H_p is the weighting matrix (related to histogram) estimating the probability density function (pdf) of the random field: BRF, GRF, or MRF; and η is an additive (Gaussian) noise field. Note that both the desired and actual contrasts may be generated as deterministic or random fields and represented in the convenient form: $\Delta T_{A,B} = \Delta \bar{T}_{A,B} + \delta(\Delta T_{A,B})$, where $\Delta \bar{T}_{A,B}$ and $\delta(\Delta T_{A,B})$ are mean values and deviations. Thus, digital linear formulation allows us to create a class of stochastic multiscale radio-brightness pictures composed of a series of random fields at varying scales and resolutions. In the case of undisturbed conditions, such pictures may reflect a stochastic ocean microwave emission background at the selected frequencies and polarizations. Alternatively, this technique allows us to generate and estimate relevant radiometric signatures related to oceanic processes and fields using methods of image processing.

4. DEMONSTRATION

We present some examples of numerical simulations of emissivities, microwave radiometric signals, images, and signatures related to variable environmental conditions.

4.1. Brief historical survey

Theory and practice show that low-contrast microwave radiometric features with $\Delta T_{Br} \sim 1\text{--}4$ K (absolute value) usually correspond to surface roughness change (referred to as “roughness signatures”), and high-contrast radiometric features with contrasts up to $\Delta T_{Br} \approx 20\text{--}30$ K correspond to oceanic two-phase dispersed media depending on their structural, electromagnetic, and coverage characteristics (referred to as “foam signatures”). Theoretically, these contrasts are calculated relative to the brightness temperature of a smooth and undisturbed water surface that doesn’t correspond to natural conditions. However, radio-brightness variations may be estimated properly using well-validated “simple” formulas developed in the early 1980s, especially for ocean passive microwave radiometry (see, e.g., [1]). Indeed, in the case of the surface roughness signatures, $\Delta T_{Br} = 2T_0 k_0^2 \int G(\vec{k}, \vec{k}_0) F(\vec{k}) d\vec{k}$, and in the case of foam signatures, $\Delta T_{Br} = T_0 \Delta \kappa_f$. Here the following designations are used: $G(\vec{k}, \vec{k}_0; \varepsilon_w)$ is the resonance function calculated analytically [19]; \vec{k} is the wave vector of the surface irregularities; \vec{k}_0 is the electromagnetic wave vector (polarization and observation parameters are defined by orientations of two wave vectors: \vec{k} and \vec{k}_0); $\varepsilon_w(\lambda; t, s)$ is the complex dielectric permittivity of seawater dependent on electromagnetic wavelength λ , temperature t , and salinity s ; $F(\vec{k}; v)$ is the two-dimensional spatial wave spectrum parameterized by wind speed v ; $\Delta \kappa_f(\lambda; t, s; d_f)$ is an increment of emissivity due to foam/whitecap/spray calculated by microwave models [4], [5]; and T_0 is the thermodynamic temperature. It has also been reported [16], [17] that the relevant radiometric signatures can be revealed in the form of monotonic trends, “smooth” deviations, and/or short-term spikes in 1-D signals; and in the form of contrast distinct spots and/or extended areas in 2-D high-resolution images. These and other important properties investigated over the years provide the physical basis for comprehensive numerical analyses and predictions of sophisticated microwave remote-sensing data.

A suggested composite model (Fig. 2) has been applied recently to compute total emissivities for a wind-driven sea surface taking into account joint impacts of many environmental factors [6]. It was assumed initially that a statistical description is the most realistic approach to deal with ocean variables. The main problem is to assign radiometric data to specified hydrodynamic phenomena having mostly stochastic and even unpredictable character. Unlike deterministic geophysical objects, scales and behavior of stochastic ocean surface events may not be known *a priori*; therefore, their reliable observations require the use of multisensor and multiresolution remote-sensing technology.

4.2. Simulations

Figs. 3, 4, and 5 illustrate a number of important realizations generated at S-L-band. Radiation-wind dependencies in terms of emissivity $\kappa(v)$ show good separability by salinity parameter (Fig. 3). The two-channel S-L-band diagram generated at $\lambda = 21$ and 6 cm (Fig. 4) represents the brightness temperature sensitivity to variations of surface temperature and salinity in terms of cluster analysis. Simulations of stochastic radiometric signals and images (Fig. 5) may also be useful to reveal types of signatures associated with a variability of surface parameters. In fact, these model data show robust microwave emission characterizations under different environmental conditions including occurrences of RSTA and, at the same time, predetermine their potential observability using S-L-band passive microwave techniques. Indeed, radiometric signals have measurable radio-brightness variations $\Delta T_B \approx -4 - +4$ K; in the corresponding images they also appear as ridges of contrast spots which may be identified by morphological (shape) criteria.

To provide a more realistic consideration, we incorporate horizontal gradients (fields) of sea surface salinity \bar{V}_s and temperature \bar{V}_t into our multifactor microwave model. In this case, considerable variations in radiometric signals and images may occur due to a stochastic spatial intermittency of different microwave contributions. Using character types of temperature-salinity gradients (linear, nonlinear) and also variable parameters of a surface-roughness spectrum, we can estimate RSTA signatures of different configuration. One schematic example is shown in Fig. 6. Input data contain three components: a) surface roughness anomaly – slick, modeled through amplitude transformations of power wave number spectrum $F(k) \sim A k^{-p}$, A and p are variable parameters; b) salinity and c) temperature surface anomalies modeled as wave-like features. Output data represent a composite microwave emission picture (d) comprising contrast objects with mosaic gradients of radio-brightness. Hypothetically, they may be perceived as relevant (RSTA) microwave radiometric signatures. Their specified texture characterization allows us to provide their detection and recognition.

5. CONCLUSION

We reported a new class of remote-sensing signatures associated with so-called “roughness-salinity-temperature anomalies” (RSTA). These phenomena can occur in the oceans due to joint variations of surface roughness, surface salinity, and temperature. To model and evaluate possible microwave emission effects, we have developed numerical simulations based on a composite multifactor hydrodynamic-electromagnetic model. Our study has demonstrated unique properties of the generated radiometric signatures (RSTA) associated with their robust texture-statistical characterization. We believe that under certain conditions (e.g., at linear resolution $\Delta x \sim 10$ -20 km, wind speed $v < 7$ m/s, sea surface temperature $t = 10$ -20°C, and salinity $s = 25$ -35 psu), environmental RSTA may be detectable using advanced S-L-band passive microwave techniques. Our data can also be useful in context with space missions: NASA-AQUARIUS and ESA-SMOS, dedicated to the global monitoring of sea surface salinity using L-band passive microwave radiometers.

6. REFERENCES

- [1] I. V. Cherny and V. Y. Raizer, *Passive Microwave Remote Sensing of Oceans*. Chichester, U.K.: Wiley, 1998.
- [2] V. Raizer, “Modeling of roughness-salinity microwave anomalies at S and L bands,” in *Proc. IGARSS'1999*, Hamburg, Germany, 28 June - 2 July, vol. IV, pp. 2309–2311, 1999.
- [3] V. Raizer, “Modeling of sea-roughness radiometric effects for the retrieval of surface salinity at 14.3 GHz,” in *Proc. IGARSS'2001*, Sydney, Australia, 9-13 July, 2001.
- [4] V. Raizer, “Modeling of L-band foam emissivity and impact on surface salinity retrieval,” in *Proc. IGARSS'2008*, Boston, MA 6-11 July 2008.
- [5] V. Raizer, “Macroscopic foam-spray models for ocean microwave radiometry,” *IEEE Trans. Geosci. Remote Sens.*, vol. 45, no. 10, pp. 3138–3144, October 2007.
- [6] V. Raizer, “Modeling L-band emissivity of a wind-driven sea surface,” in *Proc. IGARSS'2009*, Cape Town, South Africa, 13-17 July, 2009.
- [7] K. N. Fedorov and A. I. Ginzburg, *The Near-Surface Layer of the Ocean*. VSP, Utrecht, The Netherlands, 1992.
- [8] A. Soloviev and R. Lukas, *The Near-Surface Layer of the Ocean: Structure, Dynamics, and Applications*. Springer, The Netherlands, 2006.
- [9] J. S. Turner, *Buoyancy Effects in Fluids*. Cambridge, U.K.: Cambridge University Press, 1973.
- [10] R. W. Schmitt, “Observational and laboratory insights into salt finger convection,” *Progress in Oceanography*, vol. 56, issues 3–4, pp. 419–433, March 2003.
- [11] G. I. Barenblatt, I. A. Leikin, A. S., Kazmin, et al. “Suloy in the White Sea,” *Dokl. Acad. Sci. USSR*, vol. 281, pp. 1435–1439, 1985.
- [12] V. Raizer, “Microwave radiometric scenes and images of oceanic surface phenomena,” in *Proc. IGARSS'1998*, Seattle, WA 6-10 July, vol. VI, pp. 2474–2476, 1998.
- [13] V. Raizer, “Passive microwave radiometry, fractals, and ocean dynamics,” in *Proc. IGARSS'2001*, Sydney, Australia, 9-13 July, 2001.
- [14] V. Raizer, “Statistical modeling for ocean microwave radiometric imagery,” in *Proc. IGARSS'2002*, Toronto, Canada, 24-28 June, 2002.
- [15] V. Raizer, “Validation of two-dimensional ocean microwave signatures,” in *Proc. IGARSS'2003*, Toulouse, France, 21-25 July, 2003.
- [16] V. Raizer, “Texture models for high-resolution ocean microwave imagery,” in *Proc. IGARSS'2005*, Seoul, Korea, 25-29 July, 2005.
- [17] V. Raizer, “High-resolution passive microwave-imaging concept for ocean studies,” *OCEANS, 2005. Proceedings of MTS/IEEE*, vol. 1, pp. 62–69, 2005. ISBN: 0-933957-34-3.
- [18] W. K. Pratt, *Digital Image Processing 3rd edition*. New York: John Wiley & Sons, Inc., 2001.
- [19] V. G. Irisov, “Small-slope expansion for thermal and reflected radiation from a rough surface,” *Waves in Random Media*, vol. 7, pp. 1–10, 1997.

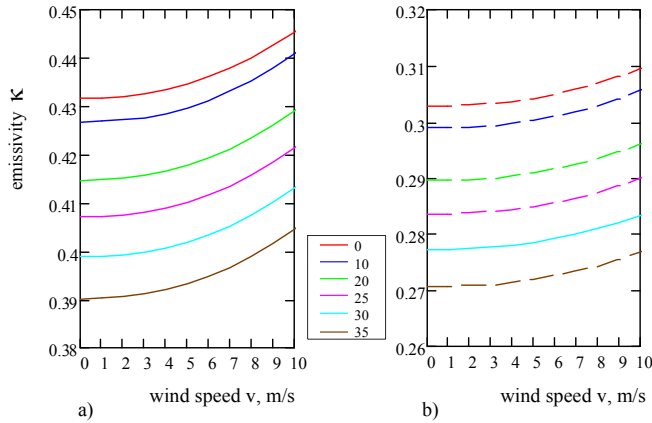


Fig. 3. Emissivity vs. wind speed calculated at L-band (1.4 GHz). (a) vertical and (b) horizontal polarizations. Incidence is 37° . Parameters of modeling: wavenumber spectrum $F(k, v) \propto A(v)k^{-4}$. Temperature $t = 10^\circ\text{C}$. Salinity is varied, $s = 0\text{--}35$ psu (marked by color).

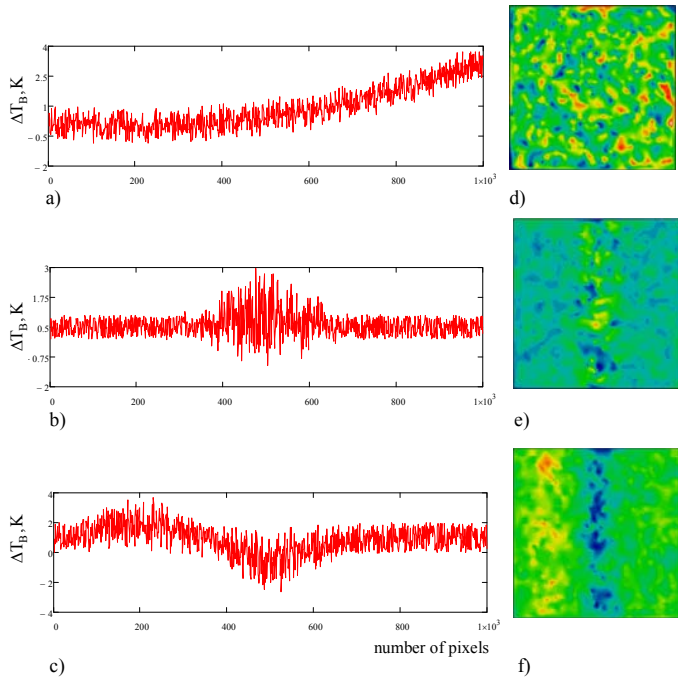


Fig. 5. Examples of simulated stochastic radio-brightness realizations – (a, b, c) signals and (d, e, f) images, related to different environmental situations. (a, d) wind action (roughness + foam), (b, e) temperature front, (c, f) surface salinity variations. Images (d, e, f) are generated from signals (a, b, c) using a Gaussian random field model. Size of simulated samples is 1024×1024 pixels.

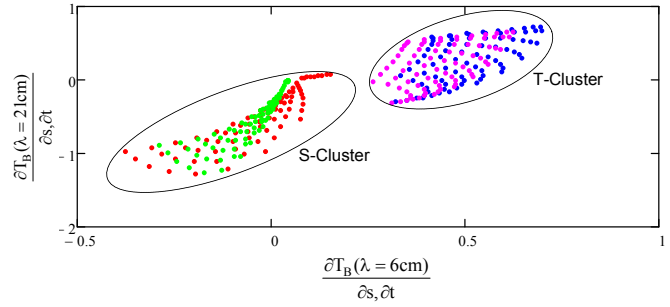


Fig. 4. Simulated two-channel S-L-band diagram of brightness-temperature sensitivities $\frac{\partial T_B(\lambda = 21\text{cm})}{\partial s, \partial t}$ vs. $\frac{\partial T_B(\lambda = 6\text{cm})}{\partial s, \partial t}$ computed for variable surface parameters. Incidence is 37° , vertical polarization. Temperature and salinity: $t = 0\text{--}40^\circ\text{C}$ and $s = 0\text{--}40$ psu. S-cluster and T-cluster are well distinguished and correspond to derivatives $\frac{\partial}{\partial s}$ and $\frac{\partial}{\partial t}$; wind speed: $v = 3$ m/s (green, purple dots) and $v = 10$ m/s (red, blue dots).

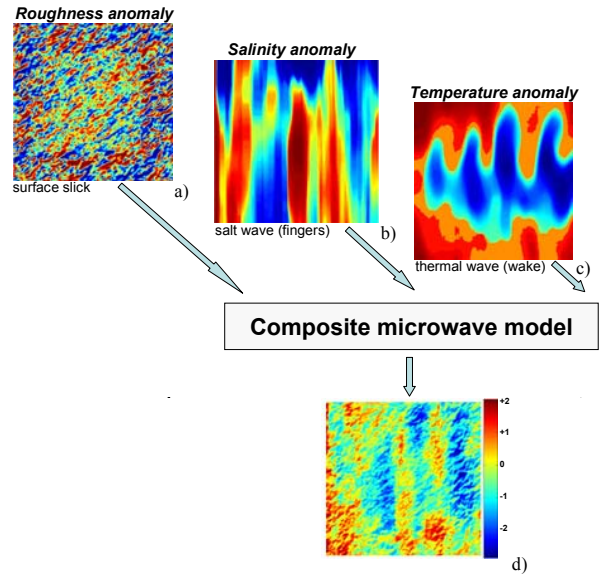


Fig. 6. Schematic illustration of oceanic RSTA simulations using three components (a, b, c). Radiometric signatures (for foam-free surface) are revealed in the resulting image (d) in the form of distinct objects with variable textures and mosaic gradients. Their observability depends on pixel resolution and averaging process. Color bar shows the radio-brightness contrast at L-band and at 37° incidence (vertical polarization).